Dynamics of colloidal aggregation in microgravity by critical Casimir forces

Potenza, M.A.C.; Manca, A.; Veen, S.J.; Weber, B.; Mazzoni, S.; Schall, P.; Wegdam, G.H.

DOI
10.1209/0295-5075/106/68005

Publication date
2014

Document Version
Final published version

Published in
Europhysics Letters

A LETTERS JOURNAL EXPLORING
THE FRONTIERS OF PHYSICS

June 2014

EPL, **106** (2014) 68005 www.epljournal.org
doi: 10.1209/0295-5075/106/68005

Dynamics of colloidal aggregation in microgravity by critical Casimir forces

M. A. C. Potenza[1], A. Manca[1], S. J. Veen[2], B. Weber[3], S. Mazzoni[4], P. Schall[3] and G. H. Wegdam[3]

[1] *Department of Physics, University of Milan - via Celoria 16, I-20133 Milan, Italy*
[2] *Unilever Research Vlaardingen - PO box 114, 3130 AC Vlaardingen, The Netherlands*
[3] *Van der Waals Zeeman Institute, University of Amsterdam - Science Park 904, 1098 XH Amsterdam, The Netherlands*
[4] *CERN - Beam Instrumentation Group - 1211 Geneva 23, Switzerland*

received 7 February 2014; accepted in final form 4 June 2014
published online 23 June 2014

PACS 82.70.Dd – Colloids
PACS 64.75.Xc – Phase separation and segregation in colloidal systems
PACS 61.43.Hv – Fractals; macroscopic aggregates (including diffusion-limited aggregates)

Abstract – By combining static and dynamic structure factor measurements under microgravity conditions, we obtain for the first time direct insight into the internal structure of colloidal aggregates formed over a wide range of particle attractions under ideal diffusion-limited conditions. By means of near-field scattering we measure the time-dependent density-density correlation function as the aggregation process evolves, and we determine the ratio of the hydrodynamic and gyration radius to elucidate the aggregate's internal structure as a function of its fractal dimension. Surprisingly, we find that despite the large variation of particle interactions, the mass is always evenly distributed in all objects with fractal dimension ranging from 2.55 for shallow potentials to 1.78 for deep ones.

Introduction. – Colloidal aggregation is important for the stability and mechanics of many complex fluids as it imparts solid-like properties to a wide range of soft materials. Most of our understanding comes from the limiting case of infinitely strong particle attraction, where particles stick irreversibly and space-spanning fractal structures [1] form at arbitrarily low particle concentration. This regime is distinct by general scaling relations for the mass distribution and robust fractal dimension. The situation is less clear at low attractive strength, where particle bonds are broken and particles can rearrange. An important question concerns the internal structure of the aggregates: weaker bonds allow particles to rearrange to reach higher density, and thus the question is how particle rearrangements at finite attraction affect the internal aggregate structure.

A lot of work in the 1980s was performed on molecular systems, theoretically and experimentally. Recently, aggregation has been studied increasingly in colloidal systems, where one can vary the interactions at will and can systematically study the resulting effect on the aggregation process. However, the disadvantage here is that the interaction cannot be varied independently of other degrees of freedom and in most cases not in a continuous fashion. We have shown that the critical Casimir effect can be used to tune the interaction just by controlling the temperature. With this effect, we could study reversible phase transitions in colloidal systems, and particle aggregation [2–4].

The open issue common to all colloidal aggregation processes is the relationship between the average size of a fractal aggregate and its Brownian diffusivity. More precisely, the relation between the radius of gyration R_g, a measure of the size of the static structure of the aggregate, and the hydrodynamic radius R_h is still not well understood. It has been shown that in the continuum regime, the ratio $\beta = R_h/R_g$ approaches a fixed value for large aggregates. This ratio is given by the internal structure or the density distribution of the aggregate. Theoretical models treating the aggregates as porous structures predict values of β between 1 and 1.2 for a fractal dimension of about 2.1, higher than experimental values. Other models give even higher values, higher by a factor of 2 and more. A discussion on these models is given in a recent paper by Pranami *et al.* [5]. They calculate the hydrodynamic and gyration radii by molecular dynamics, finding β values of 0.76 and 0.98 for fractal dimensions of 1.8 and 2.5, respectively. They compare their results with the limited number of experimental values known and find them in reasonable agreement. Their conclusion is that "*the diffusion of fractal aggregates has not yet been addressed systematically*", by varying, for example, the particle interaction. In this paper we address this issue by using the Casimir effect to vary and control the interactions. Furthermore, we will alleviate another restriction on the experiments. The experiments to date [6–9] measured ratios of R_g/R_h for Diffusion-Limited Aggregation (DLA) and Reaction-Limited Aggregation (RLA), *i.e.* in the limit of strong interaction, and in the presence of gravity. Gravity has an important effect since it not only limits the size of the aggregate, but also causes convection and sedimentation that affects the aggregation process in a decisive way. On ground, the aggregation process may start as DLA, but soon goes over into RLA, as we have shown by direct comparison of space and ground-based data [4].

In this paper we will use the description of Lin and Weitz [6] to investigate the density distribution of large fractal aggregates over a wide range of fractal dimensions, formed by ideal diffusion-limited aggregation in microgravity. For that purpose we needed a technique that measured the intermediate scattering function over a wide range of wave vectors in a single experiment. The solution was the recently introduced Near-Field Scattering (NFS) technique. In a previous publication [4] we measured the static properties of the aggregates, *i.e.* their structure factor, as the aggregation proceeds both on ground and in microgravity aboard the International Space Station (ISS). We observed that in microgravity the fractal dimension of the aggregates depended systematically on the attractive strength: The fractal dimension varied between 2.55 and 1.8. However, on ground, the aggregation was faster and a reaction-limited process led to only one type of aggregate with fractal dimension 1.65, demonstrating the essential role of gravity in the aggregation process.

Here, we provide the first experimental measurement of both R_g and R_h for fractal aggregates formed in an ideal DLA process as a function of the attractive potential, which means of the resulting fractal dimension. Three ingredients were essential for this result: the critical Casimir effect, the NFS technique, and microgravity. The first essential ingredient are the critical Casimir forces, that provide an attractive potential of controllable strength and range [3,10–18]. Critical fluctuations, in our case solvent concentration fluctuations, induce an attractive force between charge stabilized particles as the correlation length becomes of the same order of the Debye screening length. In the absence of van der Waals interactions, which are negligible in our system, the interaction between the particles can be described by a potential U that is only a function of the ratio of the correlation length, ξ, and the Debye screening length, λ_D [3,4]. The potential can thus be tuned via the temperature dependence of ξ, and it adjusts on a molecular time scale. This way, we study the aggregation process as a function of the attractive potential. NFS has been introduced some years ago in the context of fundamental studies of speckle fields [19], yielding a method to recover the far-field intensity from a simple measurement of the intensity distribution just downstream the sample [20]. The method has then been adopted for measuring colloidal aggregation [21], and has been chosen by the European Space Agency for on-board light scattering measurements thanks to the simplicity and robustness of the apparatus and the capability to measure both static and dynamic properties [22]. This allows to recover the intermediate scattering function $F(q,t)$ of the aggregates [23], and to decouple translational and rotational diffusion contributions.

The third essential ingredient is represented by the microgravity conditions at the ISS. Convection and sedimentation are absent, and pure diffusive motion of the aggregates is guaranteed. Consequently, we could follow the pure DLA process longer than ever before. From the intermediate scattering function $F(q,t)$ of the aggregates we obtain the complete static and dynamic properties of the aggregates as they are formed: we obtain the gyration radius R_g from the static structure function and the hydrodynamic radius R_h from the diffusion coefficient as a function of time. We determine the ratio $\beta = R_h/R_g$ as a function of the fractal dimension to elucidate the internal structure of the fractal objects. Surprisingly, we find that irrespectively of the bond strength and fractal dimension, the structure remains always compact, *i.e.* exhibits always a density distribution close to a unit-step function. This new degree of universality in the weak-attraction regime contrasts with previous ground measurements [6] and theoretical expectations [7] (see [5] for a recent discussion of these results compared to theoretical models). Our results are nevertheless in agreement with recent simulation results of β, obtained for two extreme values of the fractal dimension [5].

Experimental methods. – The experiment, named COLLOID, operated in the ESA Microgravity Science Glovebox, under the ELIPS program. Charge-stabilized fluorinated latex particles 400 nm in diameter, with a density of 1.6 g/mL and refractive index of $n_p = 1.37$ [24] were suspended in a mixture of 3-methyl pyridine (3MP) in water/heavy water. Weight fractions of $X_{hw} = 0.63$ for D_2O/H_2O and $X_{3MP} = 0.39$ for 3MP have been used, the solvent refractive index being 1.40. Three different suspensions were studied, each one with a colloid volume fraction of $\sim 10^{-4}$, and with different salt concentrations of 0.31, 1.5, 2.7 mmol/L of sodium chloride, corresponding to Debye screening lengths $\lambda_D = 14$ nm, 6.4 nm, and 4.8 nm, respectively. The samples were filled into quartz cells under vacuum that were tightly sealed. We used a collimated laser beam 8 mm in diameter with a wavelength of 930 nm to illuminate the sample cell, and a 0.25 NA, 20 × microscope objective to project the transmitted and scattered light onto a CCD sensor. As detailed in [4], near-field scattering images result from the interference between the intense transmitted and the (fainter) scattered light and

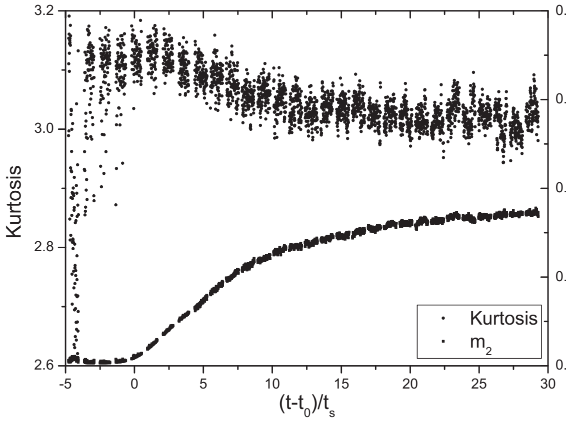

Fig. 1: Evolution of the second moment (lower curve) and the kurtosis (upper curve) during the aggregation process at the lowest attractive strength at $T = T_{agg}$. Here, we have used the reduced time $t_r = (t - t_0)/t_s$, where t_s is the time a single particle takes to diffuse over its own diameter and t_0 is the start of the aggregation process, which we define by linear extrapolation of the data to vanishing m_2.

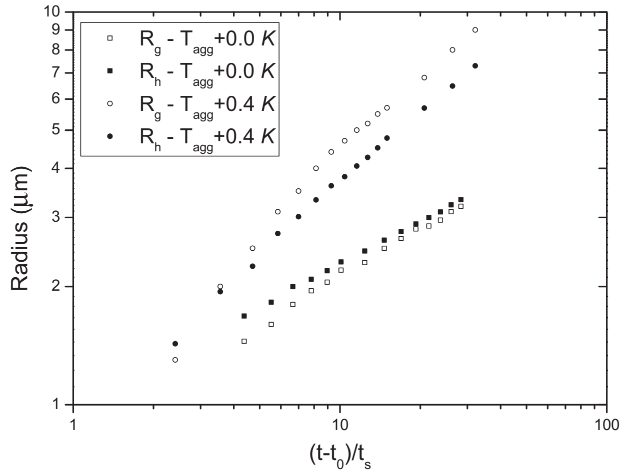

Fig. 2: Aggregate growth: evolution of R_g and R_h with time. The radius of gyration was obtained from the Fisher-Burford fit of the static power spectra. The hydrodynamic radius was obtained using eq. (2).

provide directly the scattered field-field correlation functions of the objects. We first determined the aggregation temperature, T_{agg}, by following the second moment, m_2, of the scattered intensity. We take temperature steps of 0.1 K until the value of m_2 exceeds a predefined threshold; this defines T_{agg} to within 0.1 K (see [23]). We then follow the aggregation process in time after temperature jumps from below T_{agg} to T_{agg}, $T_{agg} + 0.1, + 0.2, + 0.3$ and $+ 0.4$ K, increasing the attractive strength with each jump. For each temperature, we monitored the aggregation process for one hour by acquiring NFS images with a frame rate of $1\,\mathrm{s}^{-1}$ in batches of 100.

Results and discussion. – The growth of aggregates is reflected in the evolution of the second moment m_2 of the scattered intensity that is proportional to the cross-section and number of scatterers as shown in fig. 1. The horizontal axis shows the reduced time $t_r = (t - t_0)/t_s$, where t_s is the time a single particle takes to diffuse over its own diameter, and t_0 is the start of the aggregation process, defined by linear extrapolation of the data to vanishing m_2. Starting from t_0, the second moment rises continuously, indicating the growth of aggregates. In this regime, the m_2 curves of all samples at all temperatures can be scaled onto a single master curve, reflecting the universal growth of the aggregates. As a guide and measure of reliability, we also indicate the kurtosis, $\kappa = m_4/m_2^2$. The kurtosis varies wildly for $t_r < 0$. At these early times, subcritical nuclei may form and evaporate on the time scale of observation. For $t_r > 0$, but smaller than ~ 8, the kurtosis varies gradually, and approaches its constant value of ~ 3. For $t_r > 0$ the kurtosis does not oscillate so much, and we can measure a reliable radius of gyration and diffusion coefficient of the scattering objects.

Microgravity conditions allow unique measurement of the internal structure of the aggregates: they permit the slow Brownian motion of large aggregates to be measured, without disturbance by sedimentation or convection. The NFS measurement technique then allows us to measure the intermediate scattering function $F(q,t)$ instantaneously with respect to the much slower aggregation and diffusion processes. This provides us with the simultaneous measurement of two radii: the hydrodynamic radius, R_h, from the dynamic, and the gyration radius, R_g, from the static structure factor, allowing us to elucidate the density distribution of the growing aggregates. We have determined the gyration radius as described in [23], by fitting the data to the well-known Fisher-Burford expression [25] that links the measured form factor $S(q)$ to the aggregates' size and fractal dimension, d_f. The resulting evolution of R_g is shown by open symbols in fig. 2. In good approximation, R_g grows as a power law, $R_g \sim t_r^{1/d_f}$, as expected for a pure DLA process. Also shown is the hydrodynamic radius R_H. We obtain values of R_H from the time decay of $F(q,t)$ following the scheme by Lin *et al.* [6]. As is well known [26], the field-field correlation function of a system of monodisperse spherical objects is described by a decreasing exponential, $F(q,t) = S(q)e^{-t/\tau_0}$, with a time constant τ_0 ultimately related to the hydrodynamic radius R_h by the Stokes-Einstein diffusion coefficient $D_0 = \frac{k_bT}{6\pi\eta R_h}$, with η the solvent viscosity. The intermediate scattering function $F(q,t)$ is commonly measured by dynamic light scattering for fixed wave vector, q. Near-field scattering allows simultaneous dynamic light scattering measurement for a wide range of q, enabling us to measure $F(q,t)$ simultaneously for all accessible wave vectors.

For fractal aggregates, the decay of $F(q,t)$ is affected by the internal density distribution: their shape and polydispersity. The additional rotational degrees of freedom of objects with internal structure lead to a faster decay of $F(q,t)$, and an additional dependence on q arises in the measured, effective diffusion coefficient. To account for these rotational degrees of freedom, we define a class of spherical symmetries that determines how much an object needs to rotate before it decorrelates. The higher the symmetry, the smaller the angle and thus the time needed to decorrelate the field [6,27]. Because the rotational symmetry is connected to the scale-invariant structure factor $S(q)$ characterized by qR_g, qR_g determines uniquely the deviations from the simple case of spherical particles.

Following [6], we introduce the effective diffusion coefficient, $\tau = 1/D_{eff}q^2$ that we define from the measured decay time τ of $F(q,t)$. We then relate D_{eff} to D via the static structure factor $S(q)$ using

$$\frac{D_{eff}}{D} = 1 + \frac{1}{2\beta^2}\left[1 + \frac{3\partial \ln S(qR_g)}{\partial (qR_g)^2}\right], \tag{1}$$

For the structure factor, we use the Fisher-Burford form for monodisperse fractal aggregates $S(q,R_g) = \left(1 + (2/3d_f)q^2R_g^2\right)^{-d_f/2}$ [4,23,25]. This allows us to rewrite eq. (1) in the following form:

$$2\left(\frac{R_h}{R_g}\right)^2\left(\frac{D_{eff}}{D(R_h)} - 1\right) = \frac{2(qR_g)^2}{3d_f + 2(qR_g)^2}, \tag{2}$$

where we have separated static and dynamic quantities. The right-hand side is defined solely by the static data; it provides a master curve dependent on the product qR_g. The left-hand side is defined from the dynamic data in terms of D_{eff} and $D(R_h) = \frac{k_bT}{6\pi\eta R_h}$. We determine effective diffusion coefficients D_{eff} from the exponential time decay of F, and the temperature-dependent viscosity separately by dynamic light scattering. Taking R_g from the static data, the only free parameter is the hydrodynamic radius. To determine it, we define $f(R_h)$ that equals the left- and right-hand side of eq. (2), and we adjust R_h so that $f(R_h)$ from the dynamic data provides the best fit to the master curve.

Figure 3 shows a comparison of the light scattering data and the master curve according to eq. (2) (dashed curve), where we distinguish early and late stages of the aggregation by closed and open symbols, respectively. Here, we have considered the weakest interaction potential. The experimental data shows good agreement with the dashed curve in the late stages of aggregation. At early stages, however, larger deviations occur, which we associate with the polydispersity of aggregates. To account for it, we considered the polydispersity of aggregates explicitly following [6,7]. We assume the size distribution for fractal aggregates $N(M) = \frac{N_T}{\langle M\rangle}\left[1 - \frac{1}{\langle M\rangle}\right]^{M-1}$, where N_T is the total number of clusters, M is the cluster mass and $\langle M\rangle$ the average cluster mass. We then calculate the effective structure factor from the weighted average of the structure factors of the monodisperse objects [6,28], and the right side of eq. (2) becomes

$$f(R_h) = \frac{\sum_M N(M)M^2S(qR_g(M))\frac{2(qR_g(M))^2}{3d+2(qR_g(M))^2}}{\sum_M N(M)M^2S(qR_g(M))}. \tag{3}$$

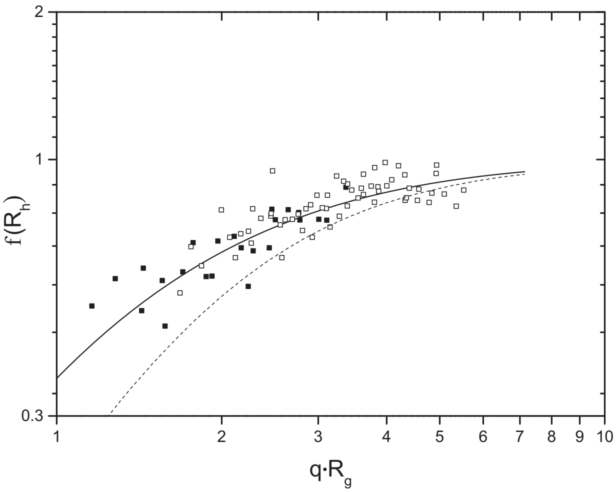

Fig. 3: Master curve according to eq. (3) (solid line) for aggregates growing by diffusion-limited aggregation at the lowest attractive strength at $T = T_{agg}$. Closed and open symbols indicate measurement results at early ($t_r < 8$) and late stages ($t_r > 8$). For comparison, the master curve according to eq. (2) is reported (dashed line).

Here we have included the explicit dependence of R_g on M that has been evaluated following the usual fractal law, $M = (R_g/a)^{d_f}$ (see [4] for a discussion on the validity of this relation in our experiment).

The resulting curve for polydisperse aggregates yields an accurate fit over the entire range of qR_g (solid line in fig. 3). Especially at later stages, the data is well fitted with one consistent value of $\beta = R_h/R_g = 1.05$. At early stages some deviations occur (closed symbols at small qR_g, t_r between 0 and 8) and the ratio R_h/R_g appears not to be constant, similar to the kurtosis: fitting the early-stage data to the polydisperse master curve, we obtain ratios of β larger than 1.07, up to 1.15.

We thus conclude that the late stages where aggregates have reached sizes large enough to have well-defined internal structure provide the most reliable data to determine R_h. In this case, the difference between polydisperse and monodisperse curves also vanishes, and both curves fit the data (see fig. 3). As a matter of fact, we find that for the later stages, the resultant values of R_h are in agreement with the monodisperse case to within 2–3%. These large aggregate sizes can only be reached in microgravity, demonstrating that microgravity measurements are essential to measure a reliable internal structure of the aggregates.

Fits of similar quality are obtained for all other interaction potentials. Thus, we have obtained the hydrodynamic radius upon the growth of the aggregates for a large range of sizes. The resulting values of R_h as a function of time are indicated by closed symbols in fig. 2. Comparison with R_g shows that the ratio R_h/R_g becomes indeed constant for larger aggregates, again for $t_r > 8$.

By considering only sufficiently large aggregates that have a well-defined fractal dimension and structure, we can now elucidate the internal structure as a function of the attractive potential and fractal dimension. We plot the ratio $\beta = R_h/R_g$ as a function of d_f in fig. 4. The color coding defines the different temperature steps, and the symbols indicate the different Debye screening lengths. Raising the temperature towards the critical point T_c of the mixture deepens the attractive minimum U_{min} of the potential, and increases the attractive strength; as the attractive strength increases, we observe lower fractal dimensions. At aggregation, the attractive strength is the same for all systems and the fractal dimension is 2.3–2.4. As the temperature increases above T_{agg}, the potential deepens, the sticking probability becomes higher and the fractal dimension decreases. The results shown in fig. 4 give an answer to the question posed in [5] about the relationship between the size of the aggregates and their diffusivity. For the first time, a pure DLA colloidal aggregation process has been studied up to relatively large structures, following at the same time the size and diffusivity through simultaneous static and dynamic light scattering measurements. The results are in accordance with the expectations of [5] (see their fig. 7), where β varies between 0.76 for $d_f = 1.8$ and 0.98 for $d_f = 2.5$.

Figure 4 now allows us to elucidate the density distribution of the fractal objects defined as $r^{d_f-3} f_c(r)$, where $f_c(r)$ is a cutoff function to account for the finite size of aggregates. To interpret the values of β, we indicate the ratio β for a fully compact object with a unit-step density distribution (solid curve) as a reference. We also computed curves for fluffier objects, one with a Gaussian density profile (dashed curve), and a second with an exponential profile (dotted curve). The data lie closest to the unit step, indicating that the aggregates have fairly compact internal structure, regardless of the fractal dimension and the attractive strength.

The effect of the Debye screening length on the potential depth can be estimated as follows: In the absence of van der Waals interactions, the potential depth is only a function of the ratio of the correlation length and the Debye screening length and increases strongly with this ratio. The correlation length obeys the scaling relation: $\xi = \xi_0(T_c - T)^{-\varepsilon}$. At T_{agg}, $\xi = c\lambda_D$, where the constant c is of order 1 [4]. Assuming λ_D to be constant with temperature, we derive for the ratio the following scaling law:

$$\begin{aligned}\xi/\lambda_D &= [(T_c - T)/(T_c - T_{agg})]^{-\varepsilon}\\ &= [(T_c - T_{agg} - \Delta T)/(T_c - T_{agg})]^{-\varepsilon}.\end{aligned} \tag{4}$$

The Debye screening length defines the scale of the temperature steps by $(T_c - T_{agg})$ in the denominator; this scale increases as λ_D decreases. Hence, with the first step of 0.1 K above T_{agg} the system with the longest screening length has the deepest potential and hence the lowest fractal dimension. This trend continues for the next temperature steps. The lowest fractal dimension observed is 1.78; as this value is reached we observe saturation and a further increase in temperature step has no effect on the aggregation process.

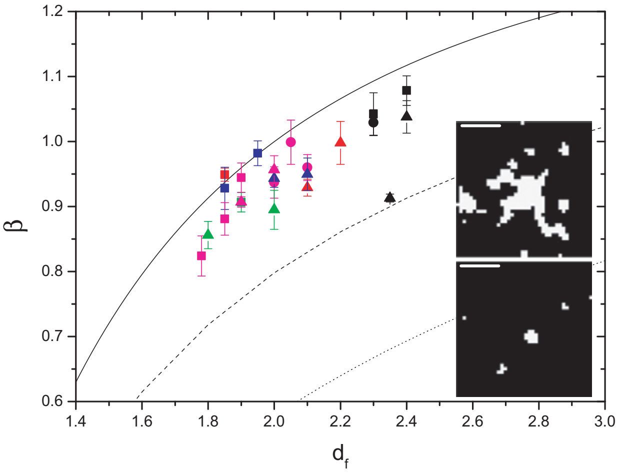

Fig. 4: (Color online) Ratio of hydrodynamic to gyration radius as a function of d_f at the temperatures $\Delta T = T - T_{agg} = 0$ (black), 0.1 (red), 0.2 (blue), 0.3 (green), and 0.4 (violet). Symbols indicate the different salt concentrations $\lambda_D = 14$ (squares), 6.4 (circles), and 4.8 nm (triangles), in the suspending liquids with salt concentrations of 0.31, 1.5, and 2.7 mmol/liter, respectively. As a reference to the β values, lines indicate the expected dependence obtained for unit-step, Gaussian and exponential density-density correlation functions (from top to bottom). Insets show holographic reconstructions of aggregates grown at $T = T_{agg} + 0.4\,\mathrm{K}$ (highest attraction, top) and $T = T_{agg}$ (lowest attraction, bottom). The length of the scale bar is 25 μm.

Besides strong changes in the attractive strength and resulting changes of the fractal dimension, however, the aggregates have surprisingly robust compact internal structure. This indicates that a certain degree of universality in the mass distribution holds, even at finite attraction. We note that the situation is very different on Earth [6,7], where β was systematically much smaller, between the lines for the exponential and Gaussian density distributions. Hence, our space measurements allow us to identify a consistent generic mass distribution in the weak-attraction regime of aggregation.

To visualize the density distribution directly, finally, we reconstruct the real-space shape of the aggregates from the near-field scattering data using holographic reconstruction. We show, as insets, results obtained by holographic reconstruction of aggregates for the smallest and largest attractive potential in the same late stage of aggregation. The irregular but compact structure of the aggregates formed at higher attractive interaction strength is clearly observable, as well as the larger size due to the higher growth rate.

In summary, for the first time we measured the structure of DLA clusters over a wide range of attractive strengths and fractal dimensions. This was possible owing to the peculiarity of the critical Casimir effect allowing us to induce tunable interactions that result in aggregates with a wide range of fractal dimensions. Microgravity guaranteed the absence of convection and the diffusion-limited growth of large clusters, whose spatial and temporal behavior could be followed over a long time span by near-field scattering that measures the intermediate structure function. Unexpectedly, the cutoff of the density correlation function does not depend on the strength of the attraction and the fractal dimension, in contrast to results obtained in ground-based experiments [6] and suggested by Wiltzius [7]. Hence, we succeeded in measuring "*the diffusion of fractal aggregates systematically*", by varying the particle interaction and thus in elucidating the internal structure or density distribution of fractal aggregates formed in an ideal diffusion-limited process.

* * *

We thank Matteo Alaimo for his help with the analysis code. This work was supported by the European Space Agency and the Dutch organization for scientific research NWO.

REFERENCES

[1] Weitz D. A. and Oliveira M., *Phys. Rev. Lett.*, **52** (1984) 1433; Aubert C. and Cannell D. S., *Phys. Rev. Lett.*, **56** (1987) 738.
[2] Guo H., Narayanan T., Sztuchi M., Schall P. and Wegdam G. H., *Phys. Rev. Lett.*, **100** (2008) 188303.
[3] Bonn D., Otwinowski J., Sacanna S., Guo H., Wegdam G. H. and Schall P., *Phys. Rev. Lett.*, **103** (2009) 156101.
[4] Veen S. *et al.*, *Phys. Rev. Lett.*, **109** (2012) 248302.
[5] Pranami G., Lamm M. H. and Vigil R. D., *Phys. Rev. E*, **82** (2010) 051402.
[6] Lin M. Y., Lindsay H. M., Weitz D. A., Klein R., Ball R. C. and Meakin P., *Phys. Rev. A*, **41** (1990) 2005.
[7] Wiltzius P., *Phys. Rev. Lett.*, **58** (1987) 710; Pusey P. *et al.*, *Phys. Rev. Lett.*, **59** (1987) 2122; Wiltzius P. and van Saarloos W., *Phys. Rev. Lett.*, **59** (1987) 2123.
[8] Wang G. M. and Sorensen C. M., *Phys. Rev. E*, **60** (1999) 3036.
[9] Katzel U., Vorbau M., Stintz M., Gottschalk-Gaudig T. and Barthel H., *Part. Part. Syst. Charact.*, **25** (2008) 19.
[10] Fisher M. E. and de Gennes P. G., *C. R. Seances Acad. Sci. Ser. B*, **287** (1978) 207.
[11] Beysens D. and Esteve D., *Phys. Rev. Lett.*, **54** (1985) 2123.
[12] Hertlein C., Helden L., Gambassi A., Dietrich S. and Bechinger C., *Nature*, **451** (2008) 172.
[13] Gambassi A. *et al.*, *Phys. Rev. E*, **80** (2009) 061143.
[14] Gnan N., Zaccarelli E., Tartaglia P. and Sciortino F., *Soft Matter*, **8** (2012) 1991.
[15] Buzzaccaro S., Colombo J., Parola A. and Piazza R., *Phys. Rev. Lett.*, **105** (2010) 198301.
[16] Gnan N., Zaccarelli E. and Sciortino F., *Nat. Commun.*, **5** (2014) 3267.
[17] Dang M. T., Vila Verde A., Nguyen V. D., Bolhuis P. G. and Schall P., *J. Chem. Phys.*, **139** (2013) 094903; Mohry T. F., Maciolek A. and Dietrich S., *J. Chem. Phys.*, **136** (2012) 224903.
[18] Nguyen D., Faber S., Wegdam G., Hu Z. and Schall P., *Nat. Commun.*, **4** (2013) 1584.
[19] Giglio M., Carpineti M. and Vailati A., *Phys. Rev. Lett.*, **85** (2000) 1416.
[20] Brogioli D., Vailati A. and Giglio M., *Appl. Phys. Lett.*, **81** (2002) 4109.
[21] Ferri F. *et al.*, *Phys. Rev. E*, **70** (2004) 041405.
[22] Magatti D., Alaimo M. D., Potenza M. A. C. and Ferri F., *Appl. Phys. Lett.*, **92** (2008) 241101.
[23] Mazzoni S. *et al.*, *Rev. Sci. Instrum.*, **84** (2013) 043704.
[24] Koenderink G. H., Sacanna S., Pathmamanoharan C., Ras M. and Philipse A. P., *Langmuir*, **17** (2001) 6086.
[25] Fisher M. E. and Burford R. J., *Phys. Rev. A*, **156** (1967) 583.
[26] Berne B. J. and Pecora R., *Dynamic Light Scattering* (Dover, New York) 2000.
[27] Lattuada M., Wu H. and Morbidelli M., *Langmuir*, **20** (2004) 5630.
[28] Manca A. *et al.*, in preparation.